Hybrid ZnAl-LDH/CNTs Nanocomposites: Noncovalent Assembly and Enhanced Photodegradation Performance

Hui Wang, Xu Xiang, and Feng Li
State Key Laboratory of Chemical Resource Engineering,
Beijing University of Chemical Technology, Beijing 100029, P.R. China

DOI 10.1002/aic.12020
Published online September 28, 2009 in Wiley InterScience (www.interscience.wiley.com).

In this article, we reported a facile and effective strategy for assembling hybrid ZnAl-layered double hydroxide/carbon nanotubes (ZnAl-LDH/CNTs) nanocomposites through noncovalent bonds, for the first time, in the presence of L*-cysteine molecules. The materials have been characterized by powder X-ray diffraction (XRD), energy dispersive X-ray spectroscopy (EDS), transmission electron microscopy (TEM), thermogravimetry and differential scanning calorimetry (TG-DSC), X-ray photoelectron spectra (XPS) and specific surface area measurement. The results indicate that* L*-cysteine as bridging linker plays a key role for enhancing both adhesion and dispersion of LDH nanocrystallites onto the surface of CNTs matrix through the interfacial interaction, and effectively inhibits the in situ growth of LDH crystallites, thus resulting in remarkably reduced LDH crystallite sizes; the Eu(III) fluorescence quenching in intercalated-Eu(III)complex LDH/CNTs nanocomposite can occur because of the interaction between LDH crystallites and CNTs matrix. Furthermore, it is found that as-assembled hybrid LDH/CNTs nanocomposites exhibit excellent performance for photodegradation of methyl orange molecules under UV irradiation, which is closely related to the unique hybrid nanostructure and composition of composites.* © 2009 American Institute of Chemical Engineers *AIChE J,* 56: 768–778, 2010
Keywords: nanocomposite, layered double hydroxide, carbon nanotube, hybrid, photodegradation

Introduction

Nowadays, considerable attention has been drawn to the water pollution which becomes more and more serious problem facing the world. Effluents discharged from industries contain many categories of dyestuffs, such as azo dyes, which are resistant to chemical decomposition and can be converted to the toxic compounds.[1,2] Up to now, photocatalysis is widely utilized to deal with pollutants in this field.[3] The use of heterogeneous prolonged-photocatalytic oxidation for wastewater treatment has been the subject of a wide range of investigations. Much attention has been paid to the photocatalytic degradation of dyes with semiconductor compounds especially like TiO_2 under UV or visible light.[4]

The assembly of carbon nanotubes (CNTs)-based heterosturctures or hybrids with the desired nanoscale guests, as an emerging and quickly developing field in the past decade, has been stimulated for tuning the properties of versatile materials and achieving a broad range of practical applications. A variety of functional materials, including metals,[5–7] semiconductors,[8] metal hydroxides or oxides,[9] and magnetic materials,[10] have been successfully assembled onto CNTs matrix by covalent[11] or noncovalent[12] interactions, which are

Additional Supporting Information may be found in the online version of this article.

Correspondence concerning this article should be addressed to F. Li at lifeng_70@163.com.

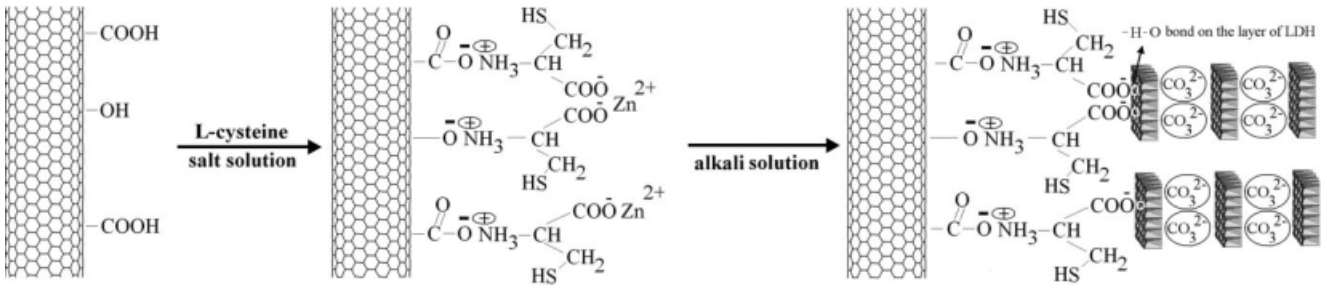

Scheme 1. Schematic illustration of the synthesis pathway for in situ growth of ZnAl-LDH onto the modified CNTs in the presence of L-cysteine.

of utmost importance to enhance affinity of guests to host CNTs. Furthermore, it is well known that CNTs are ideal and excellent support for catalytic particles, such as RuO_2,[13] Ru,[14] Pd,[15] iron oxide,[16] due to high aspect ratio, high surface area, superior chemical stability, extremely high mechanical strength, and good electronic conductivity. The common strategy for efficient assembly of nanoblocks onto CNTs is to utilize surface modification of CNTs with functional groups or reagents, which facilitates enhancing the interactions between host CNTs and guest functional materials through electrostatic force or covalent bonds.[17] However, due to the incompatibility of the crystal structure of two phases, it remains a challenge to control the assembly processes and conditions for obtaining high-quality CNT-based heterostructures or hybrids despite a lot of endeavor.

Layered double hydroxides (LDHs), also known as a family of synthetic anionic clays, consist of positively charged brucite ($Mg(OH)_2$)-like layer and charge-balancing anion (A^{n-}) in the hydrated interlayer galleries.[18,19] LDHs can be expressed by the general formula $[M^{II}_{1-x}M^{III}_x(OH)_2]^{x+}(A^{n-})_{x/n}\cdot mH_2O$, where M^{II} and M^{III} are divalent and trivalent cations, respectively, and A^{n-} represents the anions intercalated into the interlayer space together with the x value varying over a wide range. Therefore, a variety of isostructural materials with versatile physicochemical properties can be obtained by tailoring the types of cations, the molar ratios of cations and as well the types of the interlayer anions. Because of the flexible ion-exchangeability and tunable composition, LDHs have a wide range of applications as catalysts or catalyst precursors,[20–24] microcontainer, and microreactor,[25,26] additives in polymers or medicines and precursors to functional materials.[27]

It is well documented that the actually active sites participating in catalysis are located the edges of LDH platelets.[19] As the number of exposed edge sites increases with decreasing particle sizes, attempts have been made to synthesize LDHs with reduced particle sizes for improving their physicochemical activity.[28,29] On the other hand, the catalytic performance of LDHs could also be enhanced by depositing LDHs on appropriate supports with high dispersion. A number of literatures have reported on immobilization of LDH on planer or porous substrates. For example, LDH nanocrystals or nanoparticles were deposited on Si and glass substrates.[30–32] MgAl-LDH nanocrystallites were synthesized within the mesopore channels of silica material.[33] Recently, in situ growth technique has been developed for depositing LDHs on aluminum and/or alumina,[34,35] copper or zinc substrates.[36] Besides, LDHs has also reported to be randomly deposited on CNTs by a coprecipitation method.[37] The effect of host CNTs-LDH particle interaction was not studied in the work. In fact, the affinity between LDH and CNTs is unambiguously weak owing to the conventional preparation way, i.e., simple impregnation of CNTs into the starting salt solution and subsequent precipitation by alkali. Hence, there is a need for new approaches to the assembly of hybrid nanocomposites comprised of LDH nanoparticles and CNTs matrix where the dispersion of nanoparticles is uniform and stable, in order to achieve improved physicochemical performance of materials.

Herein, we develop a facile and effective approach to assemble ZnAl-layered double hydroxide (ZnAl-LDH) onto the CNTs matrix during in situ growth of ZnAl-LDH, for the first time, using L-cysteine molecule as interfacial bridging linker through noncovalent bonds. The assembly pathway of hybrid ZnAl-LDH/CNTs nanostructure is illustrated in Scheme 1. Here, nanoscale ZnAl-LDH crystallites and CNTs matrix could adhere firmly to each other via several types of functional groups in L-cysteine molecules, giving rise to hybrid ZnAl-LDH/CNTs nanocomposite with good dispersion and remarkably reduced crystallite size of ZnAl-LDH. To the best of literature knowledge, the assembly of LDH materials and CNTs in such desired and controlled noncovalent manner has not been reported. Furthermore, the photodegradation investigation revealed that as-assembled hybrid LDH/CNTs nanocomposites exhibit excellent performance for photodegradation of methyl orange molecules in aqueous solution under UV irradiation, which gives great insight into the effect of hybrid nanostructure.

Experimental

Materials

CNTs, having diameters of 40–60 nm and lengths of 5–15 μm, were purchased from Shenzhen Nanotech Port. The pristine CNTs were treated with concentrated nitric acid by refluxing them in a round-bottom flask. As a result, the hydroxyl and carboxy groups were introduced onto the surface of CNTs. And the other chemicals (analytical grade) were used as received.

Assembly of ZnAl-LDH/CNTs nanocomposites

L-cysteine (0.6058 g) along with CNTs of different weights was dissolved or dispersed into 50 ml salt solution

of $Zn(NO_3)_2$ (0.20 M) and $Al(NO_3)_3$ (0.05 M) in an ultrasonication bath for 30 min under N_2 atmosphere. Subsequently, the solution was titrated with an alkali solution of NaOH (0.4 M) and Na_2CO_3 (0.1 M) under vigorous stirring at room temperature until pH = 10.0. The suspension was aged at 333 K for 6 h. The resultant was washed with deionized water and ethanol, respectively, and then dried under vacuum at 333 K for 12 h. The obtained product was defined as LDH-cy-CNTs$_x$, in which x means the weight of CNTs added (in gram). Especially, LDH-cy-CNTs represented LDH-cy-CNTs$_{0.5}$. For comparative study, ZnAl-LDH/CNTs composite (LDH-CNTs) without addition of L-cysteine and pure ZnAl-LDH were prepared under identical reaction conditions.

Preparation of intercalated ZnAl-LDH/CNTs nanocomposites

Before the preparation of intercalated composite, the 50 ml aqueous solution containing L-cysteine (0.6058 g) and acid-treated CNTs (0.5 g) were agitated vigorously under N_2 atmosphere and dried under vacuum after filtration. The resultant product was dispersed into 50 ml salt solution of $Zn(NO_3)_2$ (0.20 M) and $Al(NO_3)_3$ (0.05 M) in an ultrasonication bath for 30 min under N_2 atmosphere. The aforementioned solution was titrated with an alkali solution of NaOH (0.4 M) and ethylene diamine-*N*,*N*-tertraacetate disodium (Na_2Y) (0.1 M) under vigorous stirring at room temperature until pH = 10.0. The suspension was aged at 333 K for 6 h. The resultant was washed with deionized water and ethanol, and then dried under vacuum at 333 K for 12 h. The intercalated-ethylene diamine-*N*,*N*-tertraacetate ZnAl-LDH/CNTs nanocomposite was defined as LDH(Y)-cy-CNTs. Europium nitrate (0.1467 g, 3.3 mmol) was dissolved in 50 ml decarbonized water containing 0.5 g LDH(Y)-cy-CNTs. The suspension was stirred at 333 K for 6 h under the atmosphere of N_2. The resultant was washed with deionized water and ethanol, and then dried under vacuum at 333 K for 12 h. The intercalated-europium(III) ethylene diamine-*N*,*N*-tertraacetate ZnAl-LDH/CNTs nanocomposite was defined as LDH(EY)-cy-CNTs. In comparison, intercalated-europium ethylene diamine-*N*,*N*-tertraacetate ZnAl-LDH, defined as LDH(EY), was also prepared with no addition of CNTs and L-cysteine under the identical conditions.

Characterization

Powder X-ray diffraction(XRD) data were collected at room temperature on Shimadzu XRD-6000 diffractometer with graphite-filtered Cu $K\alpha$ source (λ = 0.15418 nm), 40 kV, 30 mA. The samples, as unoriented powders, were step-scanned in steps of 0.040 (2θ) using a count time of 10 s/step.

Thermogravimetric (TG) and differential scanning calorimentry (DSC) analyses were carried out using a NETZSCH STA 499C thermal analysis system under argon flow at the ramping rate of 5 K/min.

The specific surface areas of samples were measured by Quantachrome Autosorb-1C-VP Analyzer using a Brunauer-Emmett-Teller (BET) method. Before measurement, samples were firstly degassed at 373 K for 2 h.

The morphology and compositions of samples were characterized by scanning electron microscopy (SEM) on a Hitachi S4700 instrument combined with energy dispersive X-ray spectroscopy (EDS).

Transmission electron microscopy (TEM) observation was carried out on a Philips FEI TECNAI-20 instrument at an accelerating voltage of 120 kV. High-resolution transmission electron microscopy was recorded on a JEM 3010 HRTEM at an accelerating voltage of 300 kV.

X-ray photoelectron spectra (XPS) was recorded on a Thermo VG ESCALAB2201-XL X-ray photoelectron spectrometer at a base pressure of 2×10^{-9} Pa using Al Kα X-ray as the excitation source.

The fluorescence spectra were recorded at room temperature by using a Shimadzu RF-5301 PC fluorescence spectrometer. The excitation source was from a Xenon lamp of 150 W.

UV–vis absorption spectra were recorded at room temperature on a Shimadzu UV-2501 PC spectrometer with an integrating sphere attachment using deionized water as background.

Photodegradation experiments

The photodegradation abilities of samples were evaluated by measuring the degradation of methyl orange (MO) in aqueous solution under UV irradiation. The UV light was irradiated from two 36 W H-type lamps with an emission maximum at 254 nm (Beijing Electric Light Sources Institute). Typically, 100 ml aqueous solution of MO (10 mg/l) containing 0.02 g solid sample was vigorously agitated for 0.5 h in the dark to reach absorption-desorption equilibrium before the irradiation. Subsequently, the suspension was irradiated under UV light. At the given time interval, 1 ml of suspension was collected to dilute to 10 ml and centrifuged to remove the solid residue. The concentration of supernatant liquid was determined by absorbance at 465 nm in UV–vis absorption spectrum to estimate the conversion of MO with irradiation time.

Results and Discussion

Assembly of hybrid ZnAl-LDH/CNTs nanocomposites

The XRD patterns of LDH-cy-CNTs, LDH-CNTs and pure ZnAl-LDH samples (Figure 1) display the characteristic reflections corresponding to hydrotalcite-like LDH family i.e., (003), (006) and (110) in each case.[38] The interlayer distance of d_{003} is ca. 0.76 nm, indicative of carbonate as charge compensating anions in the interlayer.[19] The reflection at about 26° in Figures 1b and c is assigned to the (002) reflections of graphitic carbon with a d-spacing of 0.34 nm (JCPDS No. 41-1487), which confirms the existence of CNTs. Additionally, the intensive and sharp reflections of LDH phase in the ZnAl-LDH and LDH-CNTs samples reveal high-crystalline nature and layered feature of LDH phase. In contrast, the broadened characteristic reflections of LDH-cy-CNTs composite appear almost at the same 2θ positions as those of other two samples. Furthermore, EDS analysis of LDH-cy-CNTs (Figure 2) reveals that the sample is mainly composed of C, O, and Zn elements, and the atomic ratio of Zn to Al is 3.77, very close to their feedstock ratio.

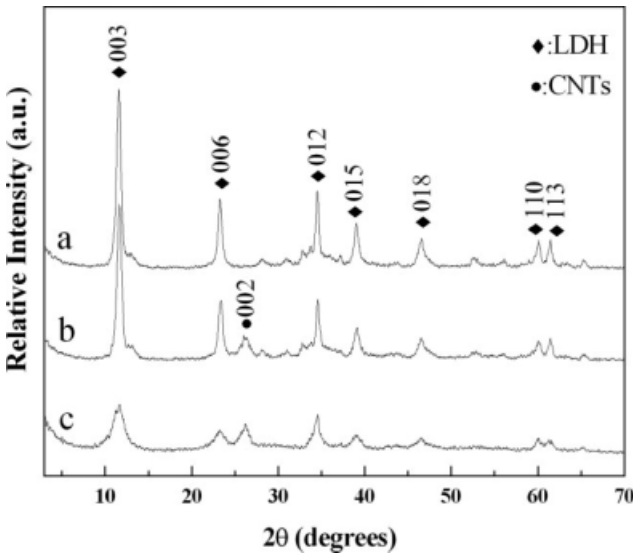

Figure 1. XRD patterns of ZnAl-LDH (a), LDH-CNTs (b) and LDH-cy-CNTs (c).

Also, the presence of the small amount of S (1.0, at. %) and N (0.8, at. %) elements confirm that L-cysteine has been introduced to LDH-cy-CNTs sample indeed.

On the other hand, the crystallite size in a and c directions for samples can be estimated from the values of full-width at half-maximum (FWHM) of the (110) reflection by means of the Scherrer formula [$L = 0.89\lambda/\beta(\theta)\cos\theta$],[38] where L is the crystallite size, λ is the wavelength of radiation used (0.15418 nm), θ is the Bragg angle, and $\beta(\theta)$ is obtained as difference of the sample width profile (FWHM) and the instrumental contribution. Therefore, the lateral crystallite sizes for ZnAl-LDH, LDH-CNTs and LDH-cy-CNTs samples are estimated to be 21.2, 16.2, and 11.6 nm, respectively (listed in Table 1). A distinct shrinkage of the crystallite sizes of LDHs in LDH-cy-CNTs sample may be attributable to the

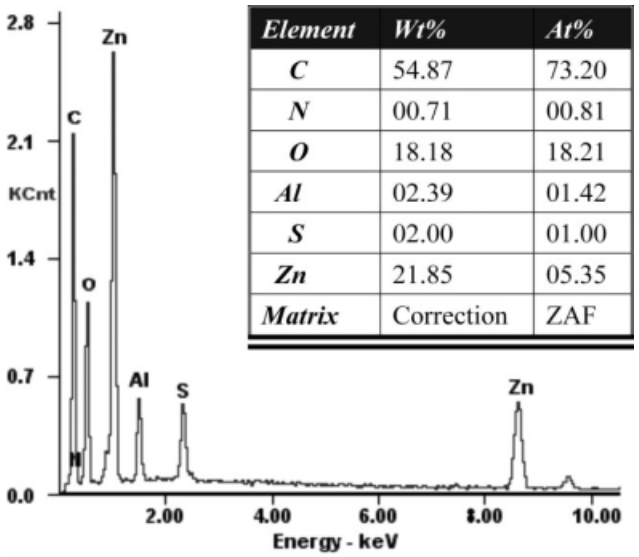

Element	Wt%	At%
C	54.87	73.20
N	00.71	00.81
O	18.18	18.21
Al	02.39	01.42
S	02.00	01.00
Zn	21.85	05.35
Matrix	Correction	ZAF

Figure 2. EDX spectrum of LDH-cy-CNTs sample.

Table 1. Indexing of XRD Patterns for Samples

Sample	d_{003} (nm)	d_{100} (nm)	Crystallite Size in a Direction (nm)	Crystallite Size in c Direction (nm)
ZnAl-LDH	0.767	0.154	21.2	13.3
LDH-CNTs	0.762	0.154	16.2	12.5
LDH-cy-CNTs	0.769	0.154	11.6	5.3
LDH(EY)	1.402	0.153	13.4	9.8
LDH(EY)-cy-CNTs	1.435	0.152	8.1	7.8

segregation and inhibition effects of L-cysteine on the growth of ZnAl-LDH crystallite onto CNTs matrix.

Usually, the interfacial bridging between two phases using functional surfactants or the compatibility of two phases is necessary to form the heterointerface. In the case of LDH/CNTs system, due to the remarkable mismatch of LDH and CNTs in the crystal structure and geometric shape, the presence of L-cysteine should play an important role in the formation of LDH/CNTs hybrid nanostructure. There are several types of functional groups, including $-NH_2$, $-COOH$, and $-SH$, within L-cysteine molecule. When mixed with the nitrate salts at an initial pH of 3.24, L-cysteine exists in the ionic form of $-(COO^-)NH_3^+$ on the basis of its pK_α value.[39] Therefore, the electrostatic interaction between $-NH_3^+$ of L-cysteine and $-COO^-$ on the modified CNTs contributes greatly to the immobilization of L-cysteine onto the surface of CNTs. On the other hand, $-COO^-$ groups of immobilized L-cysteine can selectively coordinate and/or electrostatically interact with Zn^{2+} cations in the solution. That is, L-cysteine plays a bridging linker role between CNTs and Zn^{2+} cations. Subsequently, with the successive titration of alkali, LDH nucleates in situ onto CNTs through coprecipitation process. Here, hydrogen bonding between carboxyl groups of L-cysteine and hydroxyl groups of ZnAl-LDH on the brucite-like layers further facilitates the adhesion and dispersion of ZnAl-LDH nuclei onto the surface of CNTs. As a result, the growth of ZnAl-LDH crystallites can be effectively inhibited owing to the anchoring of crystallites on the surface of CNTs matrix through L-cysteine as interfacial linker, giving thus rise to the reduced ZnAl-LDH crystallite sizes.

Generally, the thermal stability of LDH materials depends on several factors such as the nature of cations, cationic compositions, the nature of interlayer anions, the crystallinity of materials, etc.[19] Note from the TG and DSC profiles of three different samples (Figures 3 and 4) that in each case the weight loss occurs essentially in two steps, which are accompanied with two endothermic peaks.[40] The first weight loss in the temperature range from room temperature up to ca. 453 K corresponds to removal of water intercalated in the interlayer galleries of ZnAl-LDH, as well as water physisorbed on the external surface of samples, which correspondingly is related to a endothermic event in the DSC at around 423–453 K. Besides, it can be seen from Table 2 that the specific surface areas of LDH-cy-CNTs sample reaches 112 m^2/g, much larger than that of LDH-CNTs (50 m^2/g), owing to the smaller crystallite sizes of LDH confirmed by XRD. The feature of high specific surface area facilitates water molecules to absorb onto the external surface of composite.

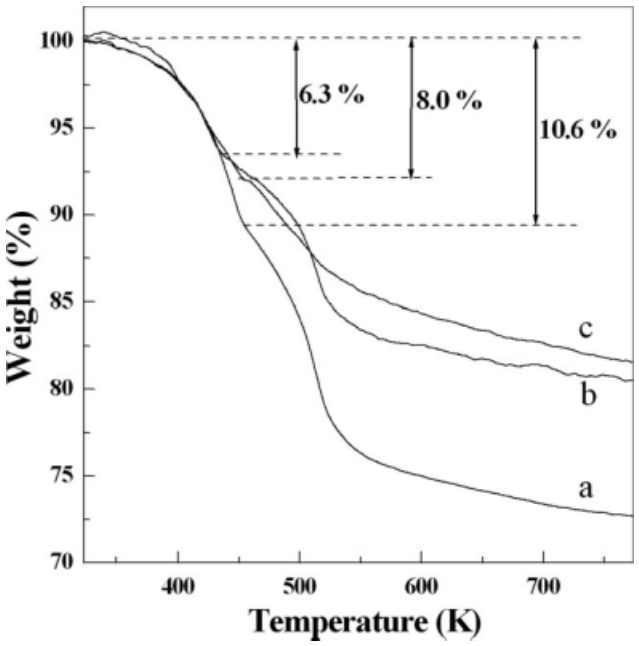

Figure 3. Thermogravimetry (TG) curves for ZnAl-LDH (a), LDH-CNTs (b), and LDH-cy-CNTs (c).

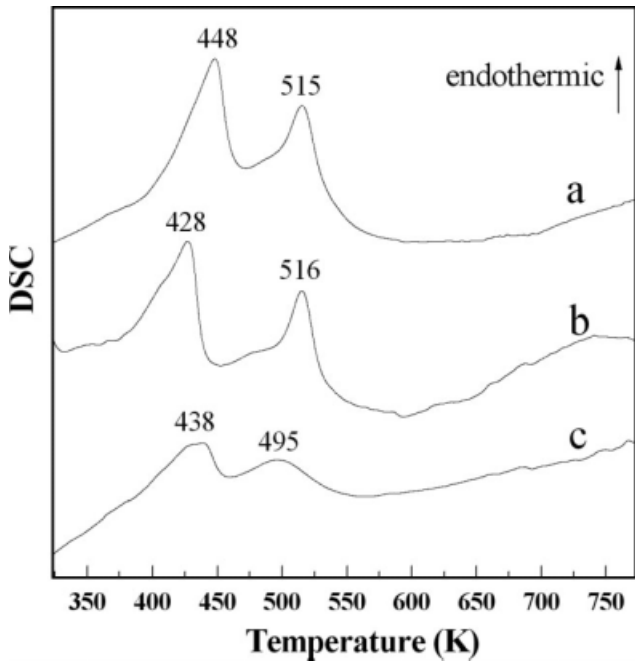

Figure 4. Differential scanning calorimetry (DSC) curves for ZnAl-LDH (a), LDH-CNTs (b), and LDH-cy-CNTs (c).

Consequently, larger weight loss (8.0%) of LDH-cy-CNTs are observed compared with those of LDH-CNTs (6.3%) during the first stage, although pristine ZnAl-LDH sample has a largest weight loss for water (10.6%) due to the absence of CNTs. In addition, owing to the hydrogen-bond interaction between adsorbed water and L-cysteine on the surface of CNTs, LDH-cy-CNTs sample displays higher endothermic peak temperature than LDH-CNTs. As for ZnAl-LDH sample, its highest endothermic peak temperature should be correlated with the dominant interlayer crystal water. The second weight loss involves dehydroxylation of the brucite-like layers and loss of volatile species arising from decomposition of the interlayer carbonate anions. This process is accompanied by an endothermic event in the DSC between 493 and 518 K. Furthermore, it is observed that there is a notable decrease in the endothermic peak temperature for composite LDH-cy-CNTs compared with other two samples, which contributes to the presence of smaller ZnAl-LDH crystallite size. It is generally accepted that when the crystallite size is reduced, the enhanced lattice deformation can lower the strength of chemical bonds in the crystal structure.[41]

Microstructure of hybrid ZnAl-LDH/CNTs nanocomposites

To achieve the information about the microstructure of as-assembled samples, TEM observations are carried out. It is clearly noted that a large amount of flake-like LDH aggregates appear in the LDH-CNTs sample (Figure 5a). Some of ZnAl-LDH crystallite aggregates are adjacent to CNTs and the other ones are isolated. Additionally, the surface of most CNTs is bare, suggestive of the poor affinity between ZnAl-LDH and CNTs. In contrast, a low-magnified TEM image of the LDH-cy-CNTs sample presents that nanosized LDH particles locate onto the surface of CNTs, and self-nucleated, isolated ZnAl-LDH nanoparticles are barely observed in the sample (Figure 5b). The surface of CNTs is discontinuously coated by ZnAl-LDH nanocrystallites. Besides, one can see from Figure 5c that a number of tiny ZnAl-LDH crystallites are sticking onto the surface of CNTs, confirming strong interaction between them. Occasionally, a few platelet-like crystallites are found inside the nanotubes, demonstrating that a small amount of feedstock can penetrate into the tubes and crystallize besides in situ growth of ZnAl-LDH on the surface of nanotubes. A high-resolution TEM observation further reveals a distinguished interfacial feature of the nanocomposite, indicative of the high affinity between the ZnAl-LDH nanoparticle and the CNTs (Figure 5d).

TEM images of as-assembled LDH-cy-CNTs$_{0.25}$ and LDH-cy-CNTs$_{0.75}$ composites with different mass ratios of CNTs (Figure 6) indicate different aggregate state of ZnAl-LDH particles onto CNTs matrix, compared with that of LDH-cy-CNTs. For LDH-cy-CNTs$_{0.25}$ with the lowest CNTs content, the dispersion of ZnAl-LDH particles is apparently poor. It is found from Figure 6a that a few ZnAl-LDH

Table 2. The Specific Surface Areas (*S*) of Samples

Sample	CNTs	ZnAl-LDH	LDH-CNTs	LDH-cy-CNTs	LDH-cy-CNTs$_{0.25}$	LDH-cy-CNTs$_{0.75}$
S (m^2/g)	61	58	50	112	50	152

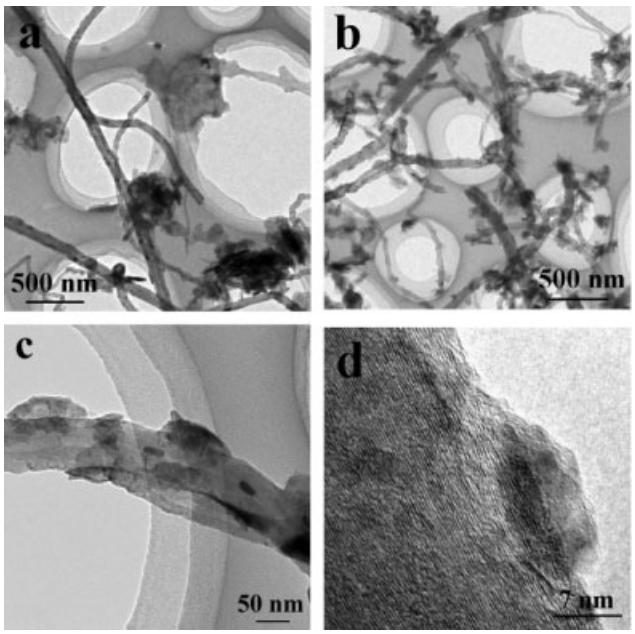

Figure 5. TEM photographs of LDH-CNTs (a) and LDH-cy-CNTs (b, c), and high-resolution TEM image of LDH-cy-CNTs (d).

particles present accumulation on CNTs owing to a small amount of CNTs, although most ZnAl-LDH particles can adhere to the surface of CNTs and separate or isolated LDH crystallites are less observed, thus resulting in the low specific surface area of LDH-cy-CNTs$_{0.25}$ (50 m^2/g), close to those of pure CNTs (61 m^2/g) and ZnAl-LDH (58 m^2/g). Here, control over the growth of ZnAl-LDH nanoparticles to obtain stable hybrid nanocomposite with uniform dispersion of ZnAl-LDH nanoparticles on CNTs are difficult. For LDH-cy-CNTs$_{0.75}$, ZnAl-LDH crystallites may be not enough to coat CNTs thoroughly due to the largest surface area of CNTs (152 m^2/g) and the highest CNTs content, but most ZnAl-LDH particles can well-dispersed on the CNTs in spite of the presence of a few isolated LDH particles. The aforementioned result demonstrates that the specific surface area increases with the CNTs content, proceeding from the improved dispersion of ZnAl-LDH particles.

The surface/near-surface chemical states of as-assembled sample are analyzed by XPS within binding energy range of 0–1200 eV (Figure 7a). The binding energy (BE) calibration of all spectra was referenced to the C 1s signal at 284.6 eV, arising from adventitious carbon for pristine LDH and sp^2-hybridized carbon of CNTs for LDH-cy-CNTs, according to the literatures.[42–44] Core levels of Zn2p, Al2p, O1s, N1s, S2p, and C1s for LDH-cy-CNTs can be identified, and no contaminant species are detectable within the sensitivity of the technique. The insert of Figure 7a for C1s spectrum was fitted with three contributions: the first one at 284.6 eV is due to the sp^2-hybridized carbon.[45] The peak at 285.9 eV is assigned to the sp^3 carbon as in disordered carbon and/or structural defect in the graphene sheets. The third one at 290.2 eV is associated to the —COO^- group. The fine spectra of Zn2p, Al2p, and O1s for LDH and LDH-cy-CNTs are displayed in Figures 7b–d, respectively. For LDH, the BE for Zn2p$_{3/2}$ locates 1022.2 eV, indicative of the presence of Zn^{2+} species.[46] And Al2p BE at 74.3 eV signifies the binding of Al—OH.[47] From the O1s spectra, it is seen that only one fitted peak at 531.8 eV appears, originating from lattice oxygen species. Compared with those for LDHs, it is noted that the BE of Zn2p, Al2p, and O1s for LDH-cy-CNTs shifts to the higher value of 1023.5, 75.6, and 533.2 eV, respectively. Such high positive BE shifts of metal and oxygen elements are similar to those reported in the case of TiO_2/CNTs composite.[44] It is known that the BE shift of elements can be associated with the chemical circumstances of elements and the BE value increases as decreasing electron density. Therefore, the shift toward higher BE for LDH-cy-CNTs is possibly ascribed to the charge transfer from the surface LDH to CNTs through L-cysteine due to the well-dispersed nature of LDH nanoparticles in the LDH-cy-CNTs and the stronger electronic interaction between LDH and CNTs. The above result confirms the role of L-cysteine as linker, which facilitates efficient interaction between LDH nanocrystallites and CNTs matrix.

To further insight the interaction between ZnAl-LDH crystallites and CNTs matrix in the type of LDH-cy-CNTs material, the fluorescence tests were carried out on $[Eu(EDTA)]^-$ complex intercalated LDH-cy-CNTs composite, LDH(EY)-cy-CNTs. As shown in Figure 8, the presence of characteristic reflection lines of LDH with (00l) and (110) harmonics indicates the two resultant samples remain layered structure. Intercalation of EuY results in an increase in interlayer spacing from 0.76 for ZnAl-LDH carbonate intercalated to 1.40 nm for LDH(EY) and 1.43 nm for LDH(EY)-cy-CNTs, as shown by the shift of (003) reflection to lower angle. It is also observed that whereas for the ZnAl-LDH(EY) sample the intensity of the (006) reflection is greater than that of the (003) reflection, the reverse is true for the EuY intercalate. This is consistent with a considerable increase in electron density in the interlayer region associated with the presence of the Eu^{3+} ions.[48] The slight weakness of I_{003}/I_{006} for LDH(EY)-cy-CNTs indicates that electron density of interlayer anion is also different from that of LDH(EY). The characteristic fluorescence peaks of Eu(III) species in LDH(EY) sample are similar to those in $[Eu(EDTA)]^-$ anions in aqueous solution by the typical characteristic photoluminescence peaks of Eu(III) with $^5D_0 \rightarrow {}^7F_i$ (i = 0–5) emission spectra and $^7F_0 \rightarrow {}^5D_2$ and $^7F_0 \rightarrow {}^5L_6$ excitation

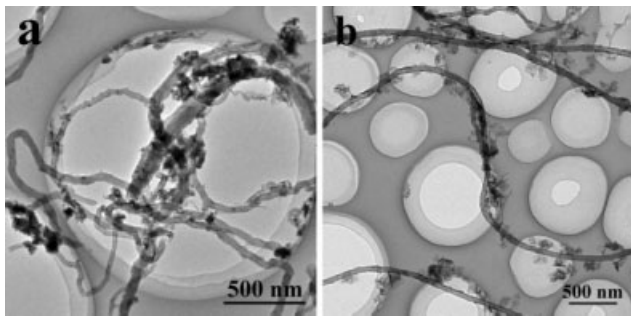

Figure 6. TEM photographs of LDH-cy-CNTs$_{0.25}$ (a) and LDH-cy-CNTs$_{0.75}$ (b).

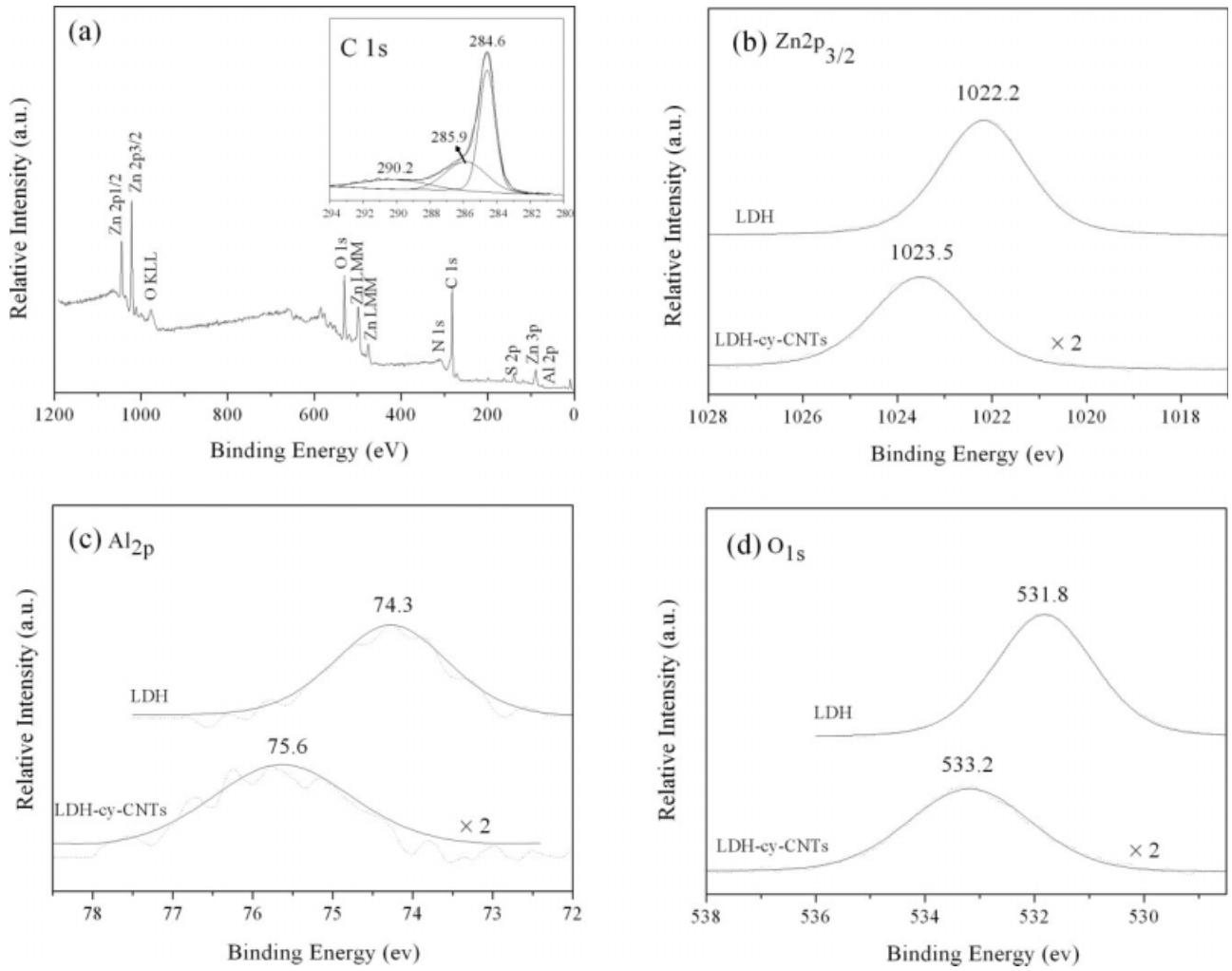

Figure 7. XPS spectra of LDH-cy-CNTs survey (insert: C1s) (a), Zn2p (b), Al2p (c), and O1s (d) of LDH and LDH-cy-CNTs.

spectra. This demonstrates that the intercalation does not affect characteristic emissions associated with Eu(III) ion. However, the fluorescence emissions of Eu(III) disappeared, whilst an emission related to CNTs appeared in LDH(EY)-cy-CNTs sample (Figure 9). The fluorescence quenching of fluorescent molecule/CNTs nanocomposites has been observed because of the energy trapping effect at the surface sites of CNTs.[49,50] Therefore, the occurrence of Eu(III) fluorescence quenching by CNTs should explicitly be correlated with strong interaction between LDH crystallites and CNTs matrix in LDH(EY)-cy-CNTs composite. However, on the basis of finding present here, the detailed study is still required to clarify the inherent relationship between the hybrid nanostructure and its fluorescence characteristic.

Photodegradation performance of ZnAl-LDH/CNTs composite

Aiming to further insight the structural uniqueness of the hybrid LDH-cy-CNTs nanocomposite, the structure-performance relationship was preliminarily investigated through photodegradation experiments of methyl orange (MO) in aqueous solution. When the suspension containing MO and ZnAl-LDH was irradiated by UV light, a discoloration phenomenon occurred. The temporal evolution of the UV–vis spectral changes taking place during the photodegradation of MO for LDH-cy-CNTs sample is displayed in Figure 10. A gradual decrease in the intensity of two strong absorption bands at 465 and 270 nm for MO solution, assigned to the azo band under the strong influence of the electron-donating dimethylamino group and the π–π^* transition related to aromatic rings,[51] respectively, can be observed during the course of the photodegradation, indicating that the azo groups and aromatic rings has been destroyed. Therefore, the significant temporal changes in the concentration of MO clearly indicate the degradation of MO in the presence of LDH-cy-CNTs nanocomposite under UV irradiation.

Figure 11 shows the degradation percentage of MO corresponding to different samples with the irradiation time. Direct photolysis in the absence of any additives brings about a decrease of 19 % in concentration after 7-h irradiation. This is because high-energy UV irradiation can lead to direct photolysis of MO molecules themselves.[52] The degradation percentage was about 55% in the presence of ZnAl-

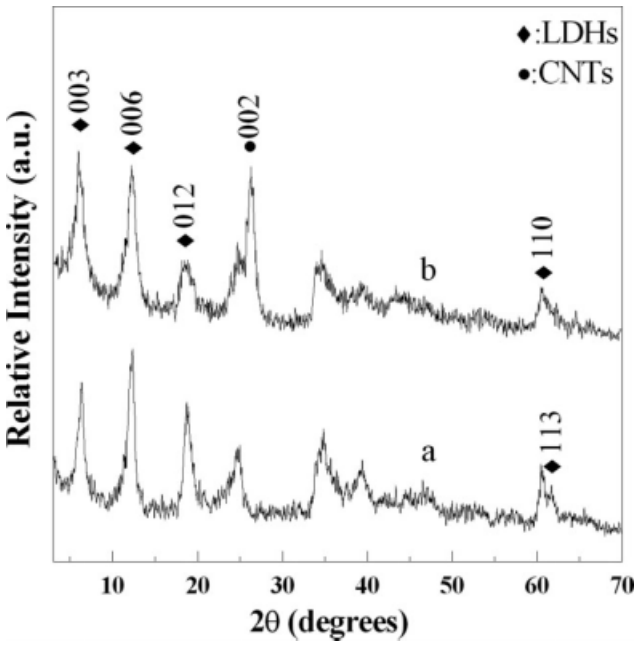

Figure 8. XRD patterns of LDH(EY) (a) and LDH(EY)-cy-CNTs (b).

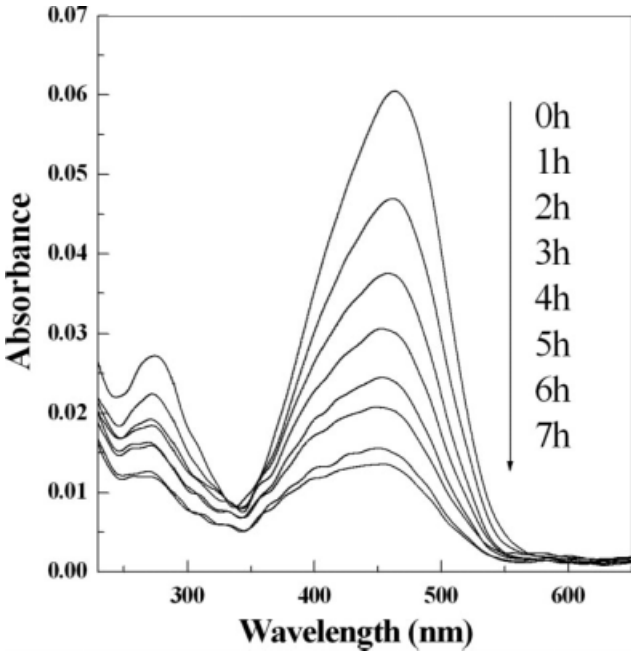

Figure 10. The temporal evolution of the UV–vis spectral changes of MO solution taking place during the photodegradation process over LDH-cy-CNTs sample under UV-light irradiation.

LDH, indicating that ZnAl-LDH can promote the degradation of MO. Because of the fact that ZnAl-LDH has no apparent absorption in the spectral region of UV irradiation, ZnAl-LDH itself does not act as an actual photocatalyst to induce the production of active radicals for degradation of MO. In fact, the ZnAl-LDH sample can absorb MO molecules in the solution, resulting thus in the increase of MO concentration in a local area. The enrichment of MO molecules on solid nanoparticles could enhance photoabsorption of sample and thus energy-induced degradation. Furthermore, the relatively large specific surface area of nanoparticles ensures full exposure of MO molecules to the UV light and

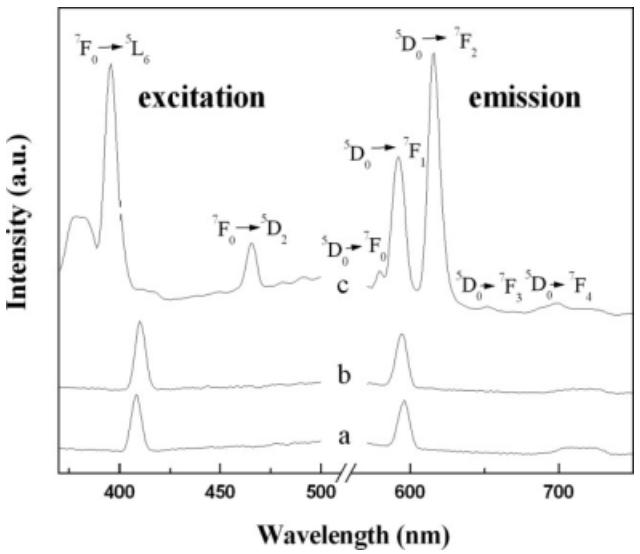

Figure 9. Fluorescence spectra of CNTs (a), LDH(EY)-cy-CNTs (b), and LDH(EY) (c) at room temperature. λ_{em} = 616 and λ_{ex} = 395 nm. (The intensities of CNTs and LDH(EY)-cy-CNTs were magnified by 10 times).

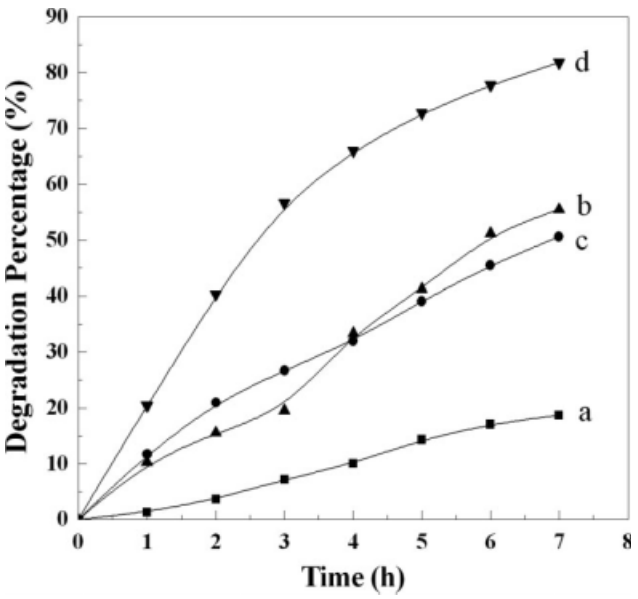

Figure 11. Degradation percentage of methyl orange with the irradiation time under UV irradiation without any additives (a), in the presence of ZnAl-LDH (b), LDH-CNTs (c), and LDH-cy-CNTs (d).

provides numerous effective sites for entrapping photons.[4] The degradation percentage of MO for LDH-CNTs sample (50%) is slightly lower than that for pristine ZnAl-LDH, although there is a large decrease of actual amount of ZnAl-LDH in LDH-CNTs sample. Further, as for LDH-cy-CNTs sample with smaller crystallite size of LDH and higher specific surface area, the degradation percentage reaches as high as 82%, due to the fact that the presence of highly dispersed ZnAl-LDH nanoparticles on the surface of CNTs matrix promotes the adsorption of MO molecules and thus enhances photoabsorption of sample. The result indicates that the unique hybrid nanostructure, where ZnAl-LDH nanoparticles can be uniformly dispersed and firmly anchored on the surface of CNTs in a given composite because of the strong interaction through interfacial bridging, plays a key role for the enhanced photodegradation performance for MO.

On the other hand, EDS analysis of the LDH-cy-CNTs sample collected after the photodegradation of MO for 7 h reveals the presence of S and N elements in the used composite catalyst, which indicates cysteine molecules still should remain in composite sample (See Supporting Information Figure 1). Also note from TEM image of used composite sample (See supporting information Figure 2) that LDH nanoparticles still adhere to the surface of CNTs, and the separated LDH particles are hardly observed. Furthermore, the LDH-cy-CNTs sample was reused and examined for the photodegradation of MO under the identical experimental conditions. It indicates that the degradation percentage reaches 81% after 7 h, almost equal to that upon the first use (See supporting information Figure 3). The aforementioned results confirm the high stability of hybrid nanostructure of LDH-cy-CNTs composite.

Concerning the effect of CNTs content in composites on degradation, the catalytic performance of LDH-cy-$CNTs_{0.25}$ and LDH-cy-$CNTs_{0.75}$ samples with different mass ratios of CNTs was investigated under the same experimental conditions. It is noteworthy that LDH-cy-$CNTs_{0.25}$ displays the fastest degradation rate and the highest degradation percentage ($\sim$93%) for MO molecules after 7 h, while the degradation percentage of LDH-cy-$CNTs_{0.75}$ with the highest CNTs content is the lowest (ca. 73%) among three composites (Figure 12). The findings indicate that the degradation efficiency of nanocomposite is improved with increasing ZnAl-LDH content. As for LDH-cy-$CNTs_{0.75}$ sample having highest surface area (Table 2), a smaller amount of LDH in nanocomposite inevitably gives rise to less adsorption sites for MO molecules, thus leading to the lower photodegradation activity. In the case of LDH-cy-$CNTs_{0.25}$, in spite of the presence of some isolated ZnAl-LDH particles grown outside CNTs and lower specific surface area, higher degradation percentage of MO molecules can be achieved due to high dispersion of a larger amount of existing ZnAl-LDH nanoparticles onto the surface of CNTs in the composite. In addition, because a few isolated LDH crystallites are found to be present in the hybrid composites in the aforementioned cases of the LDH-cy-$CNTs_{0.25}$ and LDH-cy-$CNTs_{0.75}$, they may affect the photogradation of MO to some extent.

As a result, the aforementioned result indicates that there is an important and complex factor of the hybrid nanostructure of the LDH/CNTs composites that substantially drives the efficiency of photodegradation. Apart from the principal role of the intensive interaction between LDH and CNTs in composite confirmed in this study, other qualitative parameters can include the chemical composition of the composites and the LDH nanoparticle dispersion.

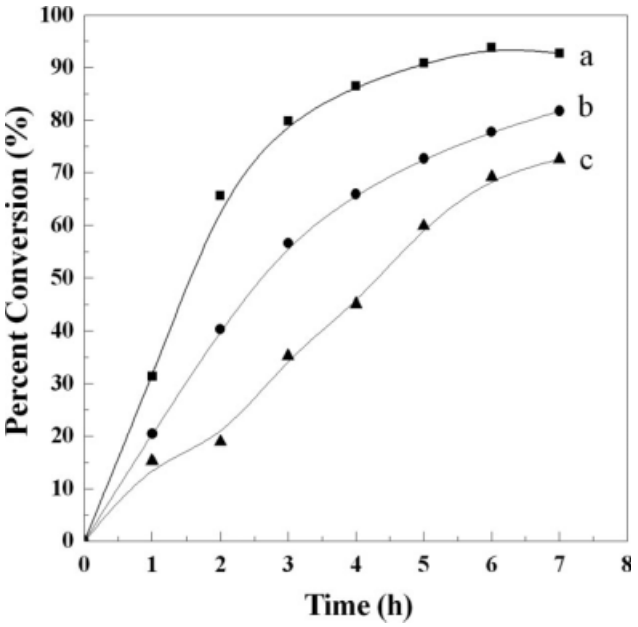

Figure 12. Degradation percentage of methyl orange with the irradiation time with LDH-cy-$CNTs_{0.25}$ (a), LDH-cy-$CNTs_{0.5}$ (b) and LDH-cy-$CNTs_{0.75}$ (c).

Conclusions

The present study provides a facile and effective approach for noncovalent assembly of hybrid ZnAl-LDH/CNTs nanocomposites with excellent photodegradation performance. The nanoscale ZnAl-LDH crystallites are uniformly dispersed and firmly anchored onto CNTs matrix, resulting from the interfacial bridging effect of L-cysteine molecule during in situ growth of ZnAl-LDH. The crystallite sizes of ZnAl-LDH in ZnAl-LDH/CNTs nanocomposites are greatly reduced in the presence of L-cysteine, indicative of its inhibiting effect on the growth of LDH crystallites. Furthermore, it is found that the photodegradation activity of as-assembled nanocomposites is dependent on their hybrid nanostructure and composition. The assembly strategy described here needs neither the participation of specialized surface chemical reactions concerned with CNTs nor complicated assembly procedure. It can be extended to various specific LDHs concerned with hybrid systems based on the prevailing CNTs materials, such as NiAl-LDH/CNTs, CoAl-LDH/CNTs and CoFe-LDH/CNTs, which are expected to exhibit the enhanced performance in catalysis, decontamination, and sensing.

Acknowledgments

The authors acknowledge the financial support from National Natural Science Foundation of China, 973 Program (2009CB939802), 111

Project (No. B07004), the Changjiang Scholars and Innovative Research Team in Universities (IRT0406) and Young Scholars Fund of Beijing University of Chemical Technology (QN0619).

Literature Cited

1. Venkatachalam N, Palanichamy M, Murugesan V. Sol-gel preparation and characterization of alkaline earth metal doped nano TiO_2: efficient photocatalytic degradation of 4-chlorophenol. *J Mol Catal A*. 2007;273:177–185.
2. Liu G, Li X, Zhao J, Hidaka H, Serpone N. Photooxidation pathway of sulforhodamine-B. dependence on the adsorption mode on TiO_2 exposed to visible light radiation. *Environ Sci Technol*. 2000;34: 3982–3990.
3. Wang J, Li R, Zhang Z, Sun W, Xie Y, Xu R, Xing Z, Zhang X. Solar photocatalytic degradation of dye wastewater in the presence of heat-treated anatase TiO_2 powder. *Environ Prog*. 2008;27:242–249.
4. Liu B, Zeng HC. Carbon nanotubes supported mesoporous mesocrystals of anatase TiO_2. *Chem Mater*. 2008;20:2711–2718.
5. Wildgoose GG, Banks CE, Compton RG. Metal nanoparticles and related materials supported on carbon nanotubes: methods and applications. *Small*. 2006;2:182–193.
6. Wang T, Hu X, Qu X, Dong S. Noncovalent functionalization of multiwalled carbon nanotubes: application in hybrid nanostructures. *J Phys Chem B*. 2006;110:6631–6636.
7. Zhang RY, Wang XM. One step synthesis of multiwalled carbon nanotube/gold nanocomposites for enhancing electrochemical response. *Chem Mater*. 2007;19:976–978.
8. Guldi DM, Aminur Rahman GM, Sgobba V, Kotov NA, Bonifazi D, Prato M. CNT-CdTe versatile donor-acceptor nanohybrids. *J Am Chem Soc*. 2006;128:2315–2323.
9. Huang Q, Gao L. Immobilization of rutile TiO_2 on multiwalled carbon nanotubes. *J Mater Chem*. 2003;13:1517–1519.
10. Korneva G, Ye H, Gogotsi Y, Halverson D, Friedman G, Bradley J-C, Kornev KG. Carbon nanotubes loaded with magnetic particles. *Nano Lett*. 2005;5:879–884.
11. Bottini M, Tautz L, Huynh H, Monosov E, Bottini N, Dawson MI, Bellucci S, Mustelin T. Covalent decoration of multi-walled carbon nanotubes with silica nanoparticles. *Chem Commun*. 2005;6:758–760.
12. Georgakilas V, Tzitzios V, Gournis D, Petridis D. Attachment of magnetic nanoparticles on carbon nanotubes and their soluble derivatives. *Chem Mater*. 2005;17:1613–1617.
13. Fu XB, Yu H, Peng F, Wang HJ, Qian Y. Facile preparation of RuO_2/CNT catalyst by a homogenous oxidation precipitation method and its catalytic performance. *Appl Catal A Gen*. 2007;321:190–197.
14. Ye XR, Lin YH, Wang CM, Engelhard MH, Wang Y, Wai CM. Supercritical fluid synthesis and characterization of catalytic metal nanoparticles on carbon nanotubes. *J Mater Chem*. 2004;14:908–913.
15. Chun YS, Shin JY, Song CE, Lee SG. Palladium nanoparticles supported onto ionic carbon nanotubes as robust recyclable catalysts in an ionic liquid. *Chem Commun*. 2008;8:942–944.
16. Chen W, Pan XL, Bao XH. Tuning of redox properties of iron and iron oxides via encapsulation within carbon nanotubes. *J Am Chem Soc*. 2007;129:7421–7426.
17. Eder D, Windle AH. Carbon-inorganic hybrid materials: the carbon-nanotube/TiO_2 interface. *Adv Mater*. 2008;20:1787–1793.
18. Evans DG, Slade RCT. Layered double hydroxides. *Struct Bond*. 2006;119:1–234.
19. Cavani F, Trifiro F, Vaccari A. Hydrotalcite-type anionic clays: preparation, properties and application. *Catal Today*. 1991;11:173–301.
20. Kapoor MP, Matsumura Y. Liquid-phase methanol carbonylation catalyzed over tin promoted nickel-aluminium layered double hydroxide. *Catal Today*. 2004;93–95:287–291.
21. Zhang F, Xiang X, Li F, Duan X. Layered double hydroxides as catalytic materials: recent development. *Catal Surv Asia*. 2008;12:253–265.
22. Hima HI, Xiang X, Zhang L, Li F. Novel carbon nanostructures of caterpillar-like fibers and interwoven spheres with excellent surface super-hydrophobicity produced by chemical vapor deposition. *J Mater Chem*. 2008;18:1245–1252.
23. Xiang X, Hima HI, Wang H, Li F. Facile synthesis and catalytic properties of nickel-based mixed-metal oxides with mesopore networks from a novel hybrid composite precursor. *Chem Mater*. 2008; 20:1173–1182.
24. Lei XD, Zhang FZ, Yang L, Guo XX, Tian YY, Fu SS, Li F, Evans DG, Duan X. Highly crystalline activated layered double hydroxides as solid acid-base catalysts. *AIChE J*. 2007;53:932–940.
25. Liu XL, Wei M, Li F, Duan X. Intraparticle diffusion of 1-phenyl-1, 2-ethanediol in layered double hydroxides. *AIChE J*. 2007;53:1591–1600.
26. Wei M, Zhang X, Evans DG, Duan X. Rh-TPPTS intercalated layered double hydroxides as hydroformylation catalyst. *AIChE J*. 2007;53:2916–2924.
27. Zou L, Xiang X, Fan J, Li F. Single-source precursor to complex metal oxide monoliths with tunable microstructures and properties: the case of Mg-containing materials. *Chem Mater*. 2007;19:6518–6527.
28. Roelofs JCAA, Lensveld DJ, Van Dillen AJ, De Jong KP. On the structure of activated hydrotalcites as solid base catalysts for liquid-phase aldol condensation. *J Catal*. 2001;203:184–191.
29. Abelló S, Medina F, Tichit D, Pérez-Ramírez J, Groen JC, Sueiras JE, Salagre P, Cesteros Y. Aldol condensations over reconstructed Mg-Al hydrotalcites: structure-activity relationships related to the rehydration method. *Chem Eur J*. 2005;11:728–739.
30. Lee JH, Rhee SW, Jung DY. Selective layer reaction of layer-by-layer assembled layered double-hydroxide nanocrystals. *J Am Chem Soc*. 2007;129:3522–3523.
31. Gardner E, Huntoon KM, Pinnavaia TJ. Direct synthesis of alkoxide-intercalated derivatives of hydrotalcite-like layered double hydroxides: precursors for the formation of colloidal layered double hydroxide suspensions and transparent thin films. *Adv Mater*. 2001; 13:1263–1266.
32. Yamaguchi N, Nakamura T, Tadanaga K, Matsuda A, Minami T, Tatsumisago M. Direct formation of Zn-Al layered double hydroxide films with high transparency on glass substrate by the sol-gel process with hot water treatment. *Cryst Growth Des*. 2006;6:1726–1729.
33. Li L, Shi J. In situ assembly of layered double hydroxide nanocrystallites within silica mesopores and its high solid base catalytic activity. *Chem Commun*. 2008;996–998.
34. Chen HY, Zhang FZ, Fu SS, Duan X. In situ microstructure control of oriented layered double hydroxide monolayer films with curved hexagonal crystals as superhydrophobic materials. *Adv Mater*. 2006; 18:3089–3093.
35. Zhang FZ, Zhao LL, Chen HY, Xu SL, Evans DG, Duan X. Corrosion resistance of superhydrophobic layered double hydroxide films on aluminum. *Angew Chem Int Ed*. 2008;47:2466–2469.
36. Liu JP, Li YY, Huang XT, Li GY, Li ZK. Layered double hydroxide nano- and microstructures grown directly on metal substrates and their calcined products for application as Li-ion battery electrodes. *Adv Funct Mater*. 2008;18:1448–1458.
37. Li C, Yao K, Liang J. Study on the features of multiwalled carbon nanotube supported nickel aluminum mixed oxides. *Appl Catal A: Gen*. 2004;261:221–224.
38. Zhao Y, Li F, Zhang R, Evans DG, Duan X. Preparation of layered double-hydroxide nanomaterials with a uniform crystallite size using a new method involving separate nucleation and aging steps. *Chem Mater*. 2002;14:4286–4291.
39. Martell AE, Smith RM, Motekaitis RJ. *NIST critically selected stability constants of metal complexes database, 7.0*. Gaithersburg, MD: U.S. Department of Commerce, 2003.
40. Theo KJ, Hickey L, Trujillano R, Jesús HM, San RMS, Rives V, Martens WN, Frost RL. Characterization of intercalated Ni/Al hydrotalcites prepared by the partial decomposition of urea. *Cryst Growth Des*. 2006;6:1533–1536.
41. Tang YJ, Li YM, Song J, Pan ZD. Structural characterization and thermal decomposition behavior of microsized and nanosized $CaCO_3$. *Acta Phys Chim Sin*. 2007;23:717–722.
42. Goh KH, Lim TT, Dong Zl. Enhanced arsenic removal by hydrothermally treated nanocrystalline Mg/Al layered double hydroxide with nitrate intercalation. *Environ Sci Technol*. 2009;43:2537–2543.
43. Lee SW, Kim BS, S Chen, Shao-Horn Y, Hammond PT. Layer-by-layer assembly of all carbon nanotube ultrathin films for electrochemical applications. *J Am Chem Soc*. 2009;131:671–679.

44. Li J, Tang SB, Lu L, Zeng HC. Preparation of nanocomposites of metals, metal oxides, and carbon nanotubes via self-assembly. *J Am Chem Soc*. 2007;129:9401–9409.
45. Yoon SM, Kim SJ, Shin HJ, Benayad A, Choi SJ, Kim KK, Kim SM, Park YJ, Kim G, Choi JY, Lee YH. Selective oxidation on metallic carbon nanotubes by halogen oxoanions. *J Am Chem Soc*. 2008;130:2610–2616.
46. Schwenzer B, Pop LZ, Neilson JR, Sbardellati TB, Morse DE. Nanostructured ZnS and CdS films synthesized using layered double hydroxide films as precursor and template. *Inorg Chem*. 2009;48: 1542–1550.
47. Gao YF, Nagai M, Masuda Y, Sato F, Seo WS, Koumoto K. Surface precipitation of highly porous hydrotalcite-like film on Al from a zinc aqueous solution. *Langmuir*. 2006;22:3521–3527.
48. Li C, Wang G, Evans DG, Duan X. Incorporation of rare-earth ions in Mg-Al layered double hydroxides: intercalation with an $[Eu(EDTA)]^-$ chelate. *J Solid State Chem*. 2004;177:4569–4575.
49. Guldi DM, Rahman GMA, Jux N, Balbinot D, Tagmatarchis N, Prato M. Multiwalled carbon nanotubes in donor-acceptor nanohybrids-towards long-lived electron transfer products. *Chem Commun*. 2005;2038–2040.
50. Alvaro M, Atienzar P, de la Cruz P, Delgado JL, Garcia H, Langa F. Sidewall functionalization of single-walled carbon nanotubes with nitrile imines: electron transfer from the substituent to the carbon nanotube. *J Phys Chem B*. 2004;108:12691–12697.
51. Galindo C, Jacques P, Kalt A. Photodegradation of the aminoazobenzene acid orange 52 by three advanced oxidation processes: UV/H_2O_2, UV/TiO_2 and VIS/TiO_2. *J Photochem Photobio A: Chem*. 2000;130:35–47.
52. Sun T, Qiu J, Liang C. Controllable fabrication and photocatalytic activity of ZnO nanobelt arrays. *J Phy Chem C*. 2008;112:715–721.

Manuscript received Apr. 1, 2009, and revision received Jun. 23, 2009.